Carbohydrate Polymers 93 (2013) 661–669

Contents lists available at SciVerse ScienceDirect

Carbohydrate Polymers

journal homepage: www.elsevier.com/locate/carbpol

Cetuximab conjugated *O*-carboxymethyl chitosan nanoparticles for targeting EGFR overexpressing cancer cells

S. Maya[a], Lekshmi G. Kumar[a], Bruno Sarmento[b,c,d], N. Sanoj Rejinold[a], Deepthy Menon[a], Shantikumar V. Nair[a], R. Jayakumar[a,*]

[a] Amrita Centre for Nanosciences and Molecular Medicine, Amrita Institute of Medical Sciences and Research Centre, Amrita Vishwa Vidyapeetham University, Kochi 682041, India
[b] Department of Pharmaceutical Technology, Faculty of Pharmacy, University of Porto, Rua Jorge Viterbo Ferreira 228, 4050-313 Porto, Portugal
[c] CICS, Health Sciences Research Center, Department of Pharmaceutical Sciences, Instituto Superior de Ciências da Saúde, Rua Central de Gandra, 1317, 4585-116 Gandra, Portugal
[d] INEB, Institute of Biomedical Engineering, University of Porto, Rua do Campo Alegre, Porto, Portugal

ARTICLE INFO

Article history:
Received 10 November 2012
Received in revised form
10 December 2012
Accepted 14 December 2012
Available online 18 January 2013

Keywords:
Carboxymethyl chitosan nanoparticles
EGFR
Targeted drug delivery
Cetuximab
Paclitaxel
Cancer nanomedicine

ABSTRACT

Nanoparticle mediated delivery of antineoplastic agents, functionalized with monoclonal antibodies has achieved extraordinary potential in cancer therapy. The objective of this study was to develop a drug delivery system comprising *O*-carboxymethyl chitosan (*O*-CMC) nanoparticles, surface-conjugated with Cetuximab (Cet) for targeted delivery of paclitaxel (PTXL) to Epidermal Growth Factor Receptor (EGFR) over-expressing cancer cells. Nanoparticles around 180 ± 35 nm and negatively charged were prepared through simple ionic gelation technique. The alamar blue assay indicated that these targeted nanoparticles displayed a superior anticancer activity compared to non-targeted nanoparticles. The nanoformulation triggered enhanced cell death (confirmed by flow cytometry) due to its higher cellular uptake. The selective uptake of Cet-PTXL-*O*-CMC nanoparticles by EGFR +VE cancer cells (A549, A431 and SKBR3) compared to EGFR −VE MIAPaCa-2 cells confirms the active targeting and delivery of PTXL via the targeted nanomedicine. Cet-PTXL-*O*-CMC nanoparticles can be used a promising candidate for the targeted therapy of EGFR over expressing cancers.

1. Introduction

Nanotherapeutics, nanoparticle based drug delivery for cancer therapy is a hot-spot in the field of medicine, which can overcome the limitations of conventional drug delivery systems. Colloidal systems such as nanoparticles offer the possibility of (a) high drug-loading efficiency with low drug leakage, (b) constant drug delivery directly to the cancer cells over an extended period, (c) enhanced therapeutic drug efficacy with negligible toxicity and (d) specific delivery of therapeutic compounds to the tumor site by enabling prolonged circulation of bioactive components by enhanced permeability and retention effect (EPR). Specific targeting ligands further increase the selectivity and efficiency of drugs to the diseased cells (Benhabbour et al., 2012; Courrier, Butz, & Vandamme, 2002; Dass & Su, 2001; Gareth, 2005; Gupta, Karar, Ramesh, Misra, & Gupta, 2010; LaVan, Lynn, & Langer, 2002; LaVan, McGuire, & Langer, 2003; Löw, Wacker, Wagner, Langer, & von Briesen, 2011; Mickler et al., 2012; Ravi Kumar, Muzzarelli, Muzzarelli, Sashiwa, & Domb, 2004; Senior, 1998). Molecular targeted therapy emerged with the aim of delivering chemotherapeutic agents specifically to the diseased target site. Bare nanocarriers can be modified by introducing ligand moieties on its surface, enabling it to target cell receptors.

Epidermal growth factor receptor (EGFR), a member of the human EGF family of receptor tyrosine kinases, is found to be over-expressed in a variety of cancer cells (Benhabbour et al., 2012; Löw et al., 2011; Mickler et al., 2012). The activation of EGFR stimulates tumor growth, proliferation, angiogenesis, invasion and metastasis. Therefore, EGFR has become a target for nanoparticle mediated cancer treatment including metastatic colorectal cancer, skin carcinoma, head and neck squamous cell carcinoma and non-small cell lung cancer (Jin et al., 2010). Recent studies have given a structural framework for a variety of agents such as monoclonal antibodies and tyrosine kinase inhibitors which effectively block the downstream signaling pathway of EGFR, thereby providing the most effective therapeutic approach for the treatment of several malignancies (Li et al., 2005; Marciniak et al., 2003; Zielinski, 2006). A number of monoclonal antibodies for blocking EGFR activation have been developed such as cetuximab (Cet), necitumumab, matuzumab and panitumumab (Pirker & Filipits, 2010; Reid, Vidal, Shaw, & Bono, 2007; Vincenzi, Schiavon, Silletta, Santini, & Tonini, 2008). Studies have shown that Cet could be used as a potential targeting ligand for therapy and targeted delivery of

* Corresponding author. Tel.: +91 484 2801234; fax: +91 484 2802020.
E-mail addresses: rjayakumar@aims.amrita.edu, jayakumar77@yahoo.com (R. Jayakumar).

0144-8617/$ – see front matter © 2012 Elsevier Ltd. All rights reserved.
http://dx.doi.org/10.1016/j.carbpol.2012.12.032

imaging agents enabling tumor characterization in vitro and in vivo (Barnard, Beauchamp, Russell, DuBois, & Coffey, 1995; Gullick, 1991; Kirkpatrick, Graham, & Muhsin, 2004; Liao, Sun, Liang, Shen, & Shuai, 2011).

Chitosan a natural, non toxic, biodegradable and biocompatible polymer has been very useful in pharmaceutical applications (Jayakumar et al., 2010; Lakshmanan, Snima, Bumgardner, Nair, & Jayakumar, 2011). *O*-CMC is a water soluble derivative of chitosan, containing —COOH and $-NH_2$ groups in the molecule and these functional groups could be exploited for biofunctionalisation with bioactive ligands (Anitha et al., 2011; Maya et al., 2012).

The aim of the present study is to evaluate the specificity and efficiency of Cet conjugated *O*-CMC nanoformulation of paclitaxel (Cet-PTXL-*O*-CMC Nps) toward EGFR overexpressing cells. Antibody conjugation was proposed to augment the therapeutic potential of PTXL-*O*-CMC nanoparticles (PTXL-*O*-CMC Nps) by promoting selective interaction with the EGFR expressed on cancer cells, thereby increasing the availability of PTXL at the target site. This targeted *O*-CMC nanosystem for PTXL delivery is described herein with focus on its synthesis, physiochemical characterization, uptake and pharmacological efficacy in cultured cells.

2. Materials and methods

2.1. Materials

O-Carboxymethyl Chitosan (*O*-CMC) (degree of deacetylation-61.8% and degree of substitution-0.54) was purchased from Koyo Chemical Co Ltd., Japan. Paclitaxel and Cet were kindly provided by Hospital de Santo António, Porto, Portugal. Calcium chloride dihydrate ($CaCl_2$) and 1-ethyl-3 (3-dimethylaminopropyl) carbodimide (EDC) were purchased from Sigma Aldrich, USA, alamar blue reagent from Invitrogen, USA and all other chemicals used were of analytical grade. The cell lines used for the study, viz. EGFR over-expressing A431 (epidermoid cancer cells), A549 (lung cancer cells), SKBR3 (breast cancer cells) and MIAPaCa-2 (pancreatic cancer cells) with lower expression of EGFR were obtained from NCCS, Pune, India. The Minimal Essential Medium (MEM) and Dulbecco Minimal Essential Medium (DMEM), Fetal Bovine Serum (FBS), Penicillin and Streptomycin used for cell culture were purchased from Sigma Aldrich, USA.

2.2. Methods

2.2.1. Preparation of PTXL-O-CMC Nps

O-CMC Nps were prepared by the simple technique of ionic gelation with varied ratios of the crosslinking cationic agent $CaCl_2$ (Anitha et al., 2009, 2011; Snima, Jayakumar, Unnikrishnan, Nair, & Lakshmanan, 2012). To the aqueous solution of *O-CMC* (0.1 wt%), 2% $CaCl_2$ was added dropwise under continuous stirring till a turbid solution was obtained. PTXL was loaded within the nanoparticles using the same method at ratio of 1.5:10.0 for PTXL:*O*-CMC. PTXL in acetone was added to 0.1 wt% *O*-CMC solution followed by $CaCl_2$ cross-linking, resulting in PTXL-*O*-CMC Nps. Drug loaded nanoparticles were separated from the unloaded drug by centrifugation for 10 min at 8500 rpm thrice and further lyophilized. The lyophilized sample was used for further characterization studies.

2.2.2. Preparation of Cet-PTXL-O-CMC Nps

Cet was conjugated to PTXL-*O*-CMC Nps using EDC activated conjugation chemistry (Deepagan et al., 2012). Carboxyl group of *O*-CMC was activated using EDC and then conjugated with the amino group of Cet. Briefly around 4 mg of nanoparticles in PBS (pH 5) was treated with 2 mg of EDC for 15 min to activate the carboxyl groups of *O*-CMC. The solution was then centrifuged at 8500 rpm for 10 min to separate activated nanoparticles, repeatedly washed to remove any unreacted EDC, and then re-dispersed in 1 mL of PBS. 2 mg/mL of Cet in PBS was added to the activated nanoparticles suspension and stirred overnight to enable antibody conjugation. The nanoparticles were then centrifuged, washed with deionized water to remove any unbound Cet and re-suspended in PBS.

To facilitate microscopic analysis of cells, Rhodamine-123 was loaded within Cet-PTXL-*O*-CMC Nps. To about 2 mL of Cet-PTXL-*O*-CMC Nps suspension in distilled water, around 30 μL of rhodamine-123 (5 mg/mL) was added and kept for overnight stirring in dark. Further it was centrifuged and the pellet was washed, re-dispersed in media and used for imaging studies.

2.2.3. Physico-chemical characterization

Size distribution and surface charge of nanoparticles before and after antibody conjugation was analyzed by dynamic light scattering (DLS) using a DLS-ZP/Particle SizerNicomp^{TM}780 ZLS equipment with suitable dilutions in water. Size and surface morphology of the nanoparticles were further confirmed by scanning electron microscope (SEM) using a JEOLJSM-6490LA (Japan) microscope. For SEM analysis, the sample was prepared by diluting nanoparticle suspension 10-fold with Millipore water before analysis and drop-casted onto metallic stubs for imaging. Fourier Transform Infrared Spectroscopy (FT-IR) was used to identify the possible interaction between various components and the nanocomplex using Perkin Elmer Spectrum RXI FTIR spectrophotometer, USA. FT-IR spectra of *O*-CMC, PTXL, Cet, PTXL-*O-CMC* Nps and Cet- PTXL-*O*-CMC Nps were recorded using Perklin Elmer Spectrum RXI Fourier Transform Infrared spectrophotometer using KBr method in the wave number range of 400–4000 cm^{-1}.

Conjugation efficiency of Cet was confirmed via BCA assay. To determine the conjugation efficiency, 200 μL of BCA reagent (50:1; Bicincioc acid:$CuSO_4$) was added to 96 well plate and then 20 μL of the Cet-PTXL-*O*-CMC NPs was added. This was further incubated for 1 h at 37 °C and the fluorescence was measured using Beckmann Coulter Elisa plate reader (BioTek Power Wave XS, UK) at 562 nm (Deepagan et al., 2012).

2.2.4. Drug encapsulation efficiency and in vitro drug release studies

PTXL encapsulation was assessed by dissolving 1 mg of nanoparticles in acetonitrile–water mixture 50:50 (v/v) to promote the total dissolution and release of the drug from the nanoparticle matrix. The nanoparticles were sonicated for 10 min and allowed to stir for 24 h for complete extraction of entrapped PTXL. The solution was further centrifuged at 8500 rpm for 10 min. PTXL was quantified spectrophotometrically at 230 nm (Agüeros, Zabaleta, Espuelas, Campanero, & Irache, 2010).

$$\text{Entrapment efficiency (\%)} = \frac{\text{amount of PTXL in the pellet}}{\text{initial amount of PTXL}} \times 100$$

In vitro PTXL release profile from *O-CMC* Nps was determined by dialysis method as described in literature (Agüeros et al., 2010) at two different pH values, 4.5 and 7.4 (Anitha et al., 2011). The nanoparticle suspension was centrifuged at 8500 rpm for 10 min and the collected pellet was re-dispersed in 2 mL of PBS. Total volume was divided equally into two and was filled in a dialysis bag. About 30 mL of PBS of pH 4.5 and pH 7.4 were placed in a beaker, the dialysis bag was introduced and kept at 37 °C with gentle stirring in a shaking incubator. The release studies were carried for different time intervals: 1, 2, 4, 6, 20, 24, 48 h up to 10 days. At proper time intervals, 1 mL from the sink was removed and replaced with fresh PBS. The amount of PTXL released at different time intervals was quantified at 230 nm using UV–vis spectroscopy. Release was

quantified based on the following equation (Li et al., 2009).

$$\text{Drug release (\%)} = \frac{\text{released PTXL at a definite time}}{\text{total amount of PTXL entrapped with in Nps}} \times 100$$

2.2.5. In vitro hemolysis assay

In vitro hemolysis assay gives an idea about the compatibility of nanoparticles for administration via systemic route. Human blood was collected from different volunteers into a tube containing anticoagulant solution consisting of acid citrate dextrose (ACD containing trisodium citrate (220 mg), citrate (8 mg) and dextrose (25 mg) in 10 mL deionised water) in the ratio (8.5:1.5). 900 μL of blood was treated with 100 μL of different concentrations of Cet-PTXL-*O*-CMC Nps and incubated for 6 h at 37 °C under gentle shaking. Then plasma was collected by centrifuging the samples at 4500 rpm for 10 min. The absorbance of the samples was determined using a spectrophotometer. Blood treated with 1% triton-X was taken as positive control and saline treated blood acted as negative control. Plasma hemoglobin concentration (mg/mL) was calculated based on the following equation (Anitha, Chennazhi, Nair, & Jayakumar, 2012; Sanoj et al., 2011).

$$\text{Plasma Hb} = \frac{[(2A_{415}) - (A_{380} + A_{450})] \times 1000 \times \text{dilution factor}}{E \times 1.655}$$

where A_{415}, A_{380} and A_{450} corresponds to the optical density values of the plasma at 380, 450 and 415 nm respectively. A_{415} is the absorption of hemoglobin based on soret band. A_{380} and A_{450} are correction factors for uroporphyrin absorption. E is molar absorptivity value of oxyhaemoglobin at 415 nm (i.e. 79.46) and 1.655 is the correction factor accounting for plasma turbidity.

$$\%\text{Hemolysis} = \frac{\text{plasma Hb value of sample}}{\text{total Hb value of blood}} \times 100$$

The nanoparticles treated blood samples were analyzed using SEM to confirm the morphology of RBC. The samples were diluted in the ratio 1:1 with saline and further fixed using glutaraldehyde for SEM analysis.

2.2.6. Cell lines and culture procedure

EGFR positive cell lines, SKBR3, A431 and A549 and MIAPaCa-2 cell lines with low expression of EGFR were maintained in DMEM supplemented with 10% fetal bovine serum and 0.5% antibiotics. The cells were incubated at 37 °C with 5% CO_2. After reaching confluence, the cells were trypsinized and subcultured in the growth medium for further studies.

2.2.7. Cell uptake studies

The differences in cellular internalization of the Cet-PTXL-*O*-CMC Nps by cancer cells with high and low EGFR expression was evaluated by fluorescent microscopy as well as flow cytometry analysis using rhodamine-123 labeled nanoparticles.

2.2.7.1. Fluorescent imaging. Cells were seeded in a density of 50,000 cells onto acid etched cover slips placed in the individual wells of a 24-well plate. After 24 h of cell attachment, the media was removed and the wells were carefully washed with PBS. Then rhodamine 123-Cet-PTXL-*O*-CMC Nps at a concentration of 0.25 mg/mL (in triplicates) was added along with media into these wells and incubated for 12 h. Further the cover slips were washed with PBS and cells were fixed in 5% paraformaldehyde followed by a final PBS wash. The cover slips were then mounted on to glass slides with DPX as the mountant and then viewed under the fluorescence microscope (Olympus DP71, USA).

2.2.7.2. Flow cytometry. The cellular uptake difference of Cet-PTXL-*O*-CMC Nps by the cancer cell lines (EGFR positive and negative cells) tracked by flow cytometry analysis. Cells were seeded in a 24 well plate at a density of 50,000 cells per well. After reaching 90% confluence, 0.25 mg/mL of rhodamine-123-Cet-PTXL-*O*-CMC Nps were added and incubated at 37 °C for 12 h. After incubation, cells were trypsinized and further analyzed via flow cytometry with excitation at 488 nm argon laser using FACS Aria II (Beckton and Dickinson, Sanjose, CA).

2.2.8. In vitro anticancer activity analysis

It is important to show the functional activity of PTXL in Cet-PTXL-*O*-CMC NPs and whether the in vitro targeted delivery of PTXL results in enhanced inhibition of cancer cell proliferation. The toxicity induced by Cet-PTXL-*O*-CMC Nps to the cancer cells were evaluated in vitro by alamar blue assay and cell viability data for cancer cells with high and low EGFR expression was collected by performing FACS via Annexin V-FITC/PI staining.

2.2.8.1. Alamar blue assay. For alamar blue assay cells were seeded in 96-well plates at the density of 10,000 cells per well and incubated for 24 h. The media was removed and the cells were then incubated with different concentration of Cet-PTXL-*O*-CMC Nps (concentration ranging from 10 to 250 μg/mL) for 24 h, followed by 4 h treatment with alamar reagent. The optical density of the solution was measured at a wavelength of 570 nm using a Beckmann Coulter Elisa plate reader (BioTek Power Wave XS). Samples were analyzed in triplicates for each experiment. The cells in media alone acted as negative control and those treated with Triton X-100 acted as positive control (Huang et al., 2012).

2.2.8.2. Cell death assay – Annexin V-FITC/PI staining. The viability of cancer cells treated with Cet-PTXL-*O*-CMC NPs were quantified by flow cytometry via Annexin V-FITC/PI Vybrant apoptosis assay kit (Molecular probes, Eugene, OR). Cells incubated with the nanoparticles for 24 h were further trypsinized, treated with the reagents and incubated in dark at room temperature for 15 min. After incubation, 400 μL of ice-cold 1× binding buffer was added, gently mixed and analyzed flow cytometrically. Here cells in media acted as negative control.

2.2.9. Statistics analysis

The experiments were carried out in triplicates and values are expressed as mean ± standard deviation (SD). A Student's *t*-test was conducted to determine the significance. A probability level of $p < 0.05$ was considered to be statistically significant.

3. Result and discussion

3.1. Preparation of Cet-PTXL O-CMC Nps

O-CMC Nps were prepared by ionic gelation technique, in which negatively charged carboxyl groups of *O*-CMC were cross-linked using $CaCl_2$. This ionic cross-linking occurs under very mild conditions, allowing a strong charge based interaction between the opposite charged groups of *O*-CMC and the cross linker (Anitha et al., 2009, 2011; Snima et al., 2012). PTXL was loaded within the Nps before the cross-linking step, after allowing the drug to interact with *O*-CMC. For cancer targeting applications, the antibody Cet, with specific EGFR affinity, was chosen as the targeting moiety because EGFR receptors are observed to be up-regulated in majority of human cancers. To aid the targeted delivery of PTXL, antibody Cet was conjugated onto the PTXL *O*-CMC Nps by EDC coupling chemistry. The preparation of Cet-PTXL-*O*-CMC Nps is outlined in Fig. 1. EDC is a water-soluble zero-length cross-linker, which is reacted

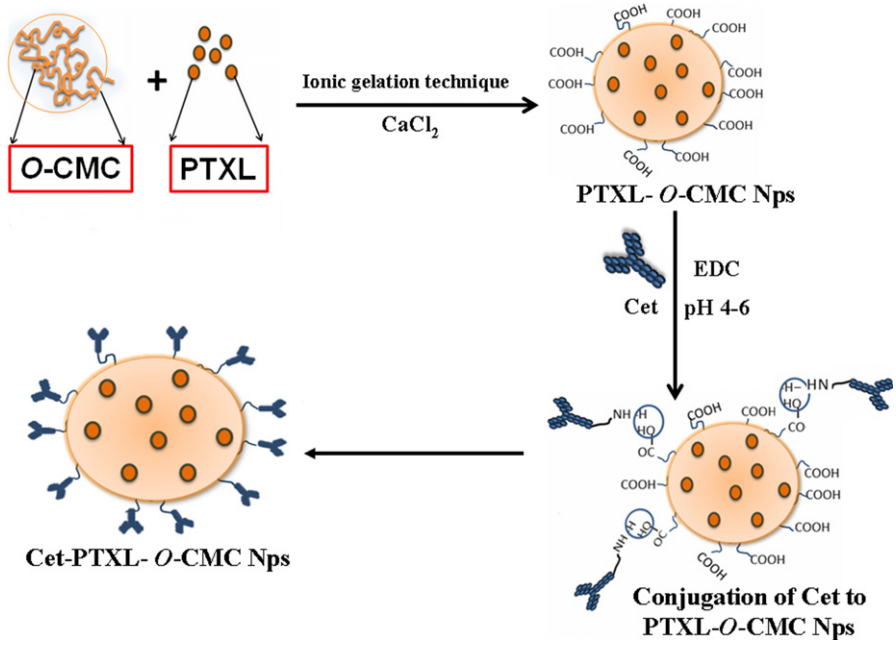

Fig. 1. Schematic illustration depicting preparation of PTXL-*O*-CMC Nps and bioconjugation of Cet on PTXL-*O*-CMC Nps through EDC activation chemistry. EDC activated the carboxyl functionality and subsequently linked to Cet through covalent linkage.

with the −COOH group of *O*-CMC at acidic pH, forming an amine-reactive *O*-acylisourea intermediate which can directly react with amines. The resultant EDC activated intermediate is reacted with the amine group of the antibody, Cet (Deepagan et al., 2012).

3.2. Physical–chemical characterization of Cet-PTXL-O-CMC nanoparticles

3.2.1. Surface morphology and size distribution

DLS experiments indicated that the mean particle size of PTXL-*O*-CMC Nps and Cet-PTXL-*O*-CMC Nps were 130 ± 25 and 180 ± 35 nm respectively. The SEM images (Fig. 2) confirmed spherical shaped nanoparticles of size range within 100 and 200 nm for *O*-CMC (Fig. 2A) and Cet-PTXL *O*-CMC Nps (Fig. 2B) respectively. The increase in size of targeted Nps when compared to the non-targeted ones is a clear indication of the surface conjugation of the antibody with the nanoparticles. The resulting size of the targeted nanoparticles is in accordance with literature for cancer drug delivery applications. It is generally accepted that the particles <200 nm tend to have prolonged circulation half-lives, escape the attack by macrophages lodged in the reticuloendothelial system and also are more favorable for passive targeting to solid tumors via the enhanced permeation and retention (EPR) effect. Cet-PTXL-*O*-CMC Nps lies within the optimal size range suitable for delivering PTXL to cancer cells (Lee, Fonge, Hoang, Reilly, & Allen, 2010).

3.2.2. Zeta potential measurements

The surface charge of the prepared nanoparticle system was analyzed by zeta potential measurements. The surface charge of the PTXL-*O*-CMC Nps was observed to be −30 ± 5 mV, which was reduced to a mean value of −12 ± 7 mV after Cet conjugation. The increase in size and the difference in zeta potential can be pointed to the surface modification occurring after Cet linkage, not only due to the high molecular weight of the antibody which provides an overall increase in diameter but also because most of the negative charges of *O*-CMC are hindered by the positive charge of Cet.

3.2.3. Chemical interaction analysis

FT-IR spectral analysis was used to study the chemical modifications occurring in the nanomatrix due to drug loading and antibody conjugation onto the Nps surface. In the FT-IR spectra (Fig. 2C), typical peaks were identified at 1632 cm^{-1} which corresponds to the N—H bending vibration band of Cet and the peak at 1734 cm^{-1} due to carbonyl stretching of *O*-CMC. PTX shows its characteristic peaks at 3935 (O-H stretching), 1631 (N—H stretching) and 1074 cm^{-1} (C—O stretching). Further in the Cet-PTXL-*O*-CMC Nps, the relevant peaks of PTXL showed a slight shift in their peaks confirming the encapsulation of PTXL. In the Cet-PTXL *O*-CMC Nps spectrum, a peak was observed at 1645 cm^{-1} confirming the formation of amide bond between *O*-CMC Nps and Cet (Anitha et al., 2009, 2011; Deepagan et al., 2012).

The presence of Cet on the surface of nanoparticles was also confirmed by BCA assay through protein estimation by recording the absorbance of the incubated solution at 562 nm. The Cet conjugation efficiency was found to be 42 ± 6%.

3.3. Entrapment efficiency and in vitro drug release profile of Cet-PTXL-O-CMC Nps

The encapsulation efficiency was determined spectrophotometrically at 230 nm by quantifying the PTXL in the supernatant after completely extracting PTXL from the Nps in acetonitrile/water mixture. It was found to be 75 ± 4%. Polymer and drug concentrations are the major factors affecting the entrapment efficiency. Higher amount of *O*-CMC allows more loading and entrapment, but resulted in large sized particles. At higher drug concentration, entrapment efficiency was reduced and drug tends to precipitate. Since antibody conjugation initially occurs at an acidic pH, some amount of PTXL loss was expected to happen, which might be the surface bound drug. However, owing to the short reaction time of only 15 min at the acidic pH, and also because the activated Nps are transferred back to neutral pH, further loss of the drug is hindered. Considering all these factors, at the optimal concentration of *O*-CMC and PTXL, an entrapment efficiency of 75 ± 4% and particle size of 200 nm was obtained.

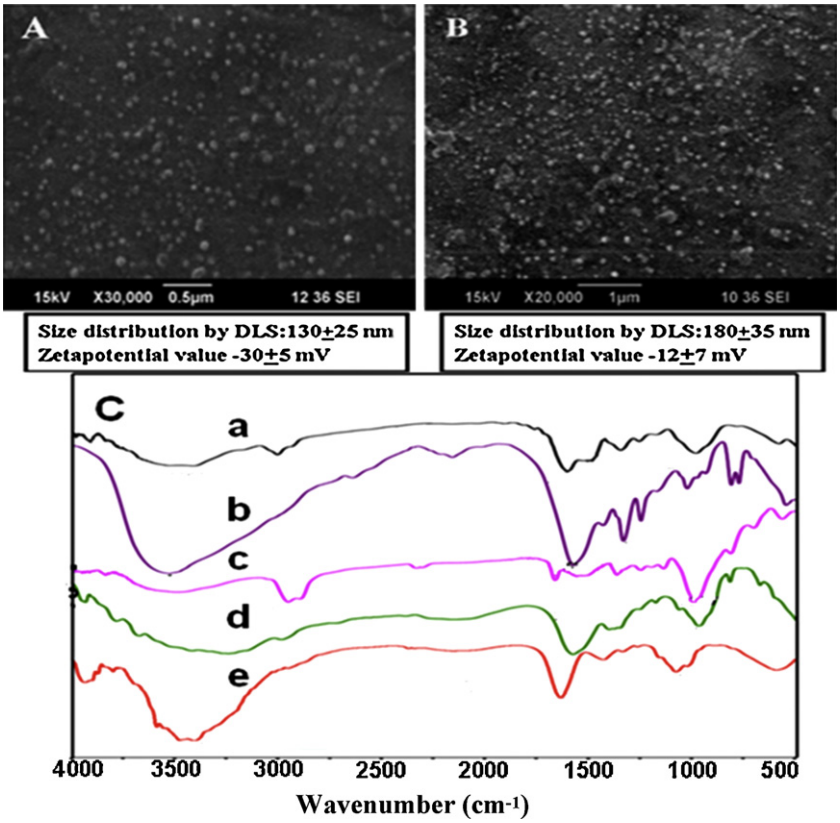

Fig. 2. Scanning electron microscopic (SEM) images (A) PTXL-*O*-CMC NPs and (B) Cet-PTXL-*O*-CMC NPs showing spherical Nps within 100–200 nm size. (C) FT-IR spectrum showing (a) Cet-PTXL-*O*-CMC Nps, (b) Cet, (c) PTXL-*O*-CMC Nps, (d) PTXL and (e) *O*-CMC.

The in vitro release of PTXL from nanoparticles was analyzed in PBS at pH 7.4 and 4.5. The result, as indicated by the drug release pattern (Fig. 3), showed an initial burst release in the first 24 h, probably due to release of surface adsorbed drug, and followed by a slower release pattern for 10 days. Cet-PTXL *O-CMC* Nps showed slow and controlled release of PTXL from the nanoparticles and higher percentage of PTXL was released at pH 4.5 than 7.4. Around 80% of the drug was released at pH 4.5 and in pH 7.4 around 50% of the drug was released after 10 days. In case of targeted drug delivery systems, after receptor mediated endocytosis the drug could be released in early or secondary endosomes by pHcontrolled hydrolysis (pH drop from physiological 7.4 – 5–6 in endosomes or 4–5 in lysosomes) or specifically by enzymolysis in lysosomes. So this could help in the enhanced release of PTXL in the tumor tissue as the extracellular pH in the tumor tissue is lower than that of the normal and also within the acidic intracellular compartments (endosomes and lysosomes) (Ulbrich & Subr, 2004). The release pattern of PTXL from the Cet conjugated nanomatrix was in a very slow rate and also pH dependant. The pH dependant release can be attributed to the swelling property of the polymer matrix. At lower pH the residual amine groups is protonated and creates a repulsive force between the adjacent positive charge thereby causing the polymer to swell and more amount of drug will be diffused out. Basic medium, unlike acidic medium limits swelling which inhibits the diffusion of drugs at a faster rate (Prabaharan, Reis, & Mano, 2007). This slow release could be attributed to the diffusion of the drug from the highly conjugated polymer matrix whose surface is tightly covered with Cet along with the slow degradation of the matrix.

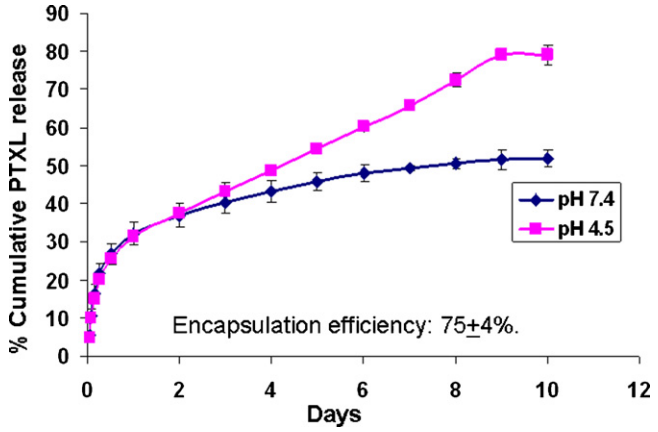

Fig. 3. Drug release profile of PTXL from Cet-PTXL-*O*-CMC Nps at pH 7.4 and pH 4.5. Around 80% of the drug was released at pH 4.5 and in pH 7.4 around 50% of the drug was released after 10 days.

3.4. Hemolysis assay

To assess the safety of administering nanoformulations via systemic route, the hemocompatability of the Nps might be understood as a value screening. Hemolysis was measured by estimating the concentration of free Hb in plasma. Fig. 4A represented the optical photographs of blood samples treated with nanoformulations showing clear plasma compared to positive control (Triton giving 100% hemolysis) with red colored plasma due to lysed RBC. Hemolysis assay (Fig. 4B) showed that the hemolytic ratio of the samples (even up to 1 mg/mL) was within the range of less than 5%, the critical safe hemolytic ratio for biomaterials according to ISO/TR 7406 (Anitha et al., 2012; Sanoj et al., 2011). These results indicate that Nps were not adversely affecting the RBC. SEM image (Fig. 4C) of the RBC showed that the nanoparticle treatments have not affected

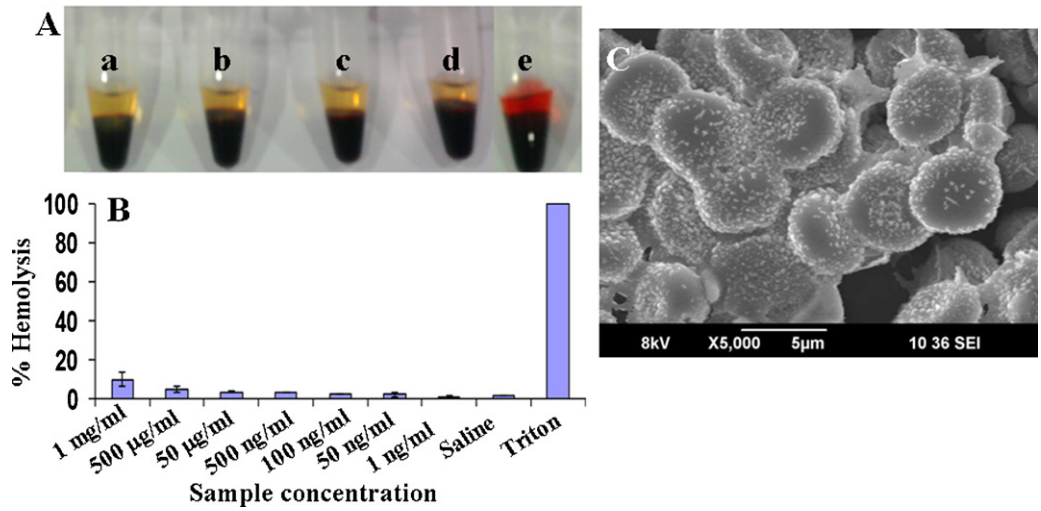

Fig. 4. (A) Photograph of Cet-PTXL-*O*-CMC Nps treated with human blood, (B) hemolysis assay graph showing %Hemolysis versus sample concentration and (C) SEM image of RBC treated with Cet-PTXL-*O*-CMC Nps. The Hemolysis assay result showed affordable hemolytic ratio and intact RBC indicating the non-hemolytic property of the Nps.

its morphology and it confirmed the non-hemolytic property of the Nps. Hemolysis is the loss of membrane integrity of red blood cells (RBCs) leading to the leakage of hemoglobin (Hb) into blood plasma. Hemolysis is one of the basic tests to understand the interaction of nanoparticles with RBCs. Nanoparticles might affect the membrane integrity of RBCs by mechanical damage. The Hemolysis assay result showed affordable hemolytic ratio and intact RBC indicating the non-hemolytic property of the nanoparticles and their safety for IV administration (Dutta & Dey, 2011).

3.5. *Cell uptake studies through flow cytometry and fluorescent microscopy*

In order to investigate the selective targeting ability of Cet-PTXL-O-CMC Nps against EGFR on the cells, A549, A431 and SKBR3 cells were employed as overexpressing EGFR and MIAPaCa-2 with low EGFR expressing cancer cells. Flow cytometry quantified the fluorescence intensity emitted from the cells that have taken up rhodamine-123 labeled nanoparticles and provided a scatter plot showing the percentage of cellular uptake. Fig. 5 shows the uptake profile of the nanoparticles by A549, A431, SKBR3 and MIAPaCa-2 cells. Rhodamine-123-Cet-PTXL-*O*-CMC Nps showed significant difference in their uptake upon interaction with treated with A549, A431 and SKBR3 cells compared to that of MIAPaCa-2 cells. Comparing the cellular uptake of targeted and non-targeted nanoparticles by the EGFR overexpressing cell lines, it can be observed that while ~75–90% of cells take up the targeted Nps, only about 20–50% cells take up the non-targeted Nps. Moreover, EGFR negative MIAPaCa-2 cells uptake less number of both targeted and non-targeted Nps. Due to the difference in the EGFR expression by the cancer cell lines, the cellular uptake of the Cet-PTXL-O-CMC Nps showed significant difference. This clearly suggests that the uptake of these Rho-Cet-PTX-*O*-CMC Nps by the cells is highly specific and receptor mediated.

Fluorescent microscopic images of actin and DAPI stained A549, A431, SKBR3 and MIAPaCa-2 cells treated with Rho-Cet-PTXL-*O*-*CMC* Nps are shown in Fig. 6. Actin dye stained the actin filaments and DAPI stained the nucleus of the cells. In the merged image, the yellowish color indicated the merging of green color of rhodamine labeled nanoparticles with that of the red color of actin, clearly indicating the uptake and internalization of the nanoparticles by EGFR positive A549, A431 and SKBR3 cells. In contrast MIAPaCa-2 (low EGFR) cells showed negligible fluorescence indicating the absence of non specific targeting. The internalization of the nanoparticles by EGFR over-expressing cancer cells indicated the targeting ability of antibody conjugated nanoparticles. Thus, the receptor mediated cellular uptake of targeted Cet-PTXL-O-CMC Nps by the tumor cells is well observed. Thus, higher cellular binding with eventual uptake as observed by microscopic and flow cytometric analysis in the case of targeted nanoparticles is presumably by receptor mediated endocytosis (Bareford & Swaan, 2007).

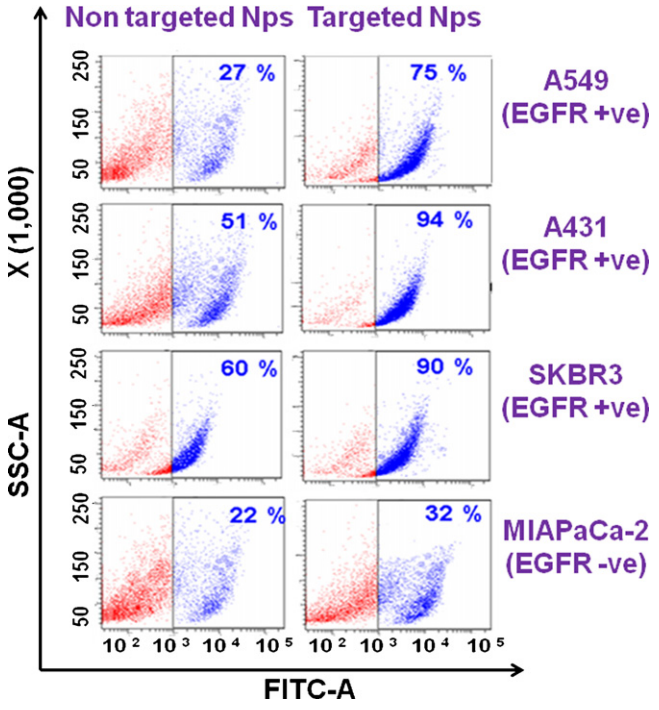

Fig. 5. Cellular uptake studies of rhodamine-123 labeled Cet-PTXL-*O*-CMC NPs by flow cytometry. Typical flow cytometric graphs of cells after 12 h incubation with both targeted (Cet-PTXL-*O*-CMC Nps) and non targeted (PTXL-*O*-CMC Nps) nanoparticles labeled with rhodamine-123. A549, A431 and SKBR4 (EGFR overexpressing) cells enhanced cellular uptake compared to MIAPaCa-2 (lower expression of EGFR) cells.

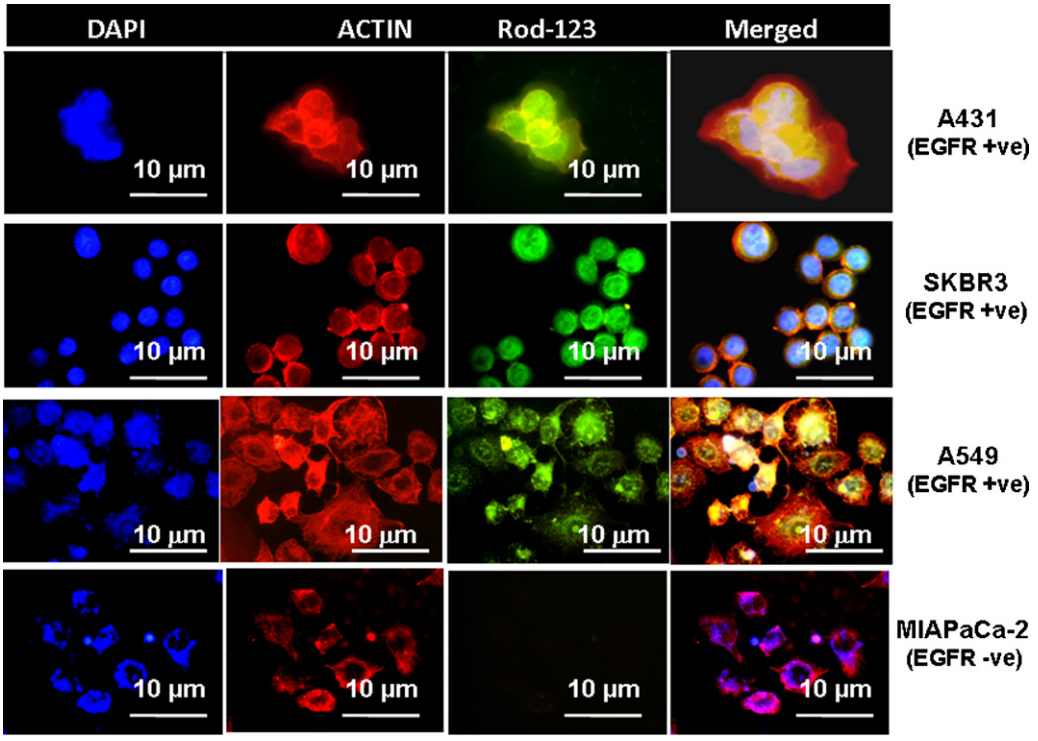

Fig. 6. Fluorescence microscopic analyses of the cellular uptake rhodamine-123 labeled Cet-PTXL-*O*-CMC Nps by cancer cells expressing different levels of EGFR. Cells after 12 h incubation with the nanoparticles are stained with actin and DAPI and visualized under fluorescent microscope under suitable filters to differentiate actin filaments and nucleus. Actin, DAPI, rhodamine-123 and the merged images are represented.

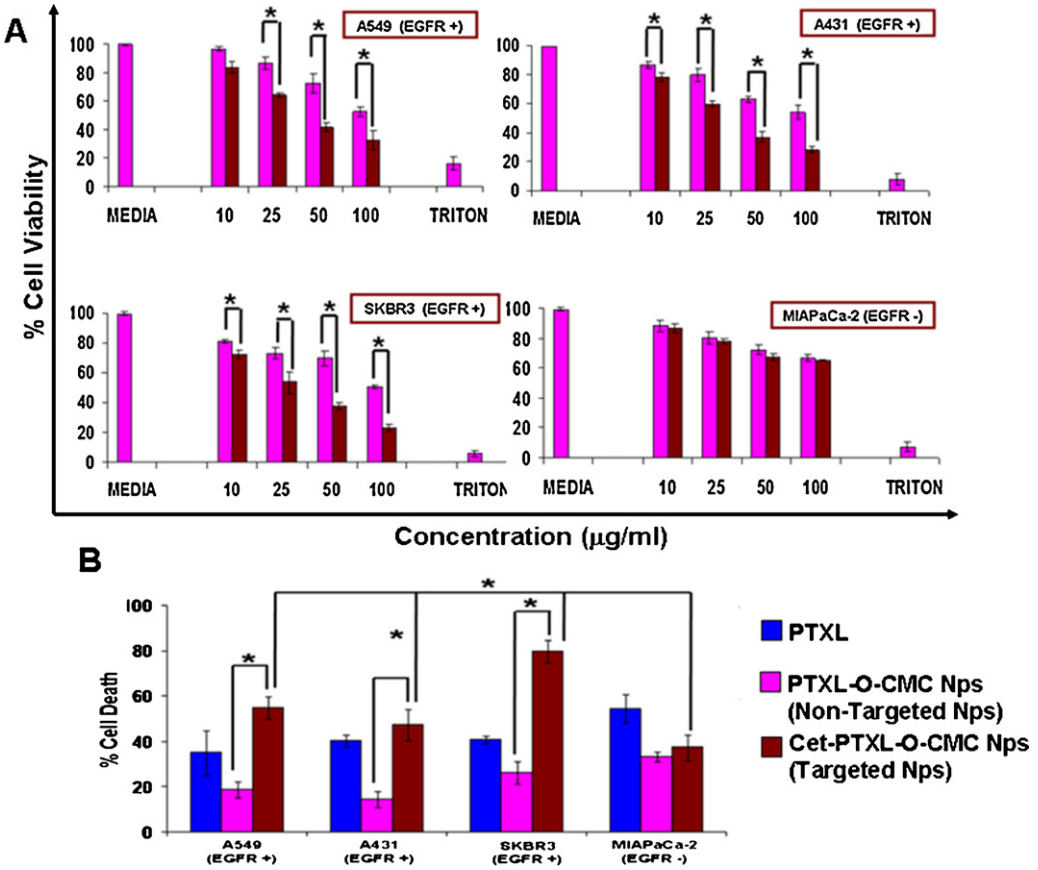

Fig. 7. In vitro anticancer activity. (A) Cell viability plot of A549, A431, SKBR3 and MIAPaCa-2 cells by alamar blue assay after 24 h incubation with Cet-PTXL-*O*-CMC Nps and PTXL-*O*-CMC Nps of different concentration. (B) Flow cytometric analysis of cancer cell death by Annexin V/PI assay in A549, A431, SKBR3 and MIAPaCa-2 cells when exposed to bare PTXL, PTXL-*O*-CMC Nps and Cet-PTXL-*O*-CMC Nps for 24 h.

3.6. In vitro anticancer activity analysis

One of the major limitations of hydrophobic therapeutic agents is their reduced bioavailability and short half life. A targeted nanoformulation of hydrophobic drugs helps to improve the drug bioavailability and provide enhanced cytotoxic effects to target cells. The cytotoxicity induced by PTXL-*O*-*CMC* Nps and Cet-PTXL-*O*-*CMC* Nps was evaluated by using alamar blue assay for 24 h. The non-toxicity of the nanocarrier (*O*-CMC NPs) as such has already been reported (Anitha et al., 2011). The cell viability plots (Fig. 7A) of A549, A431 and SKBR3 cells showed a higher toxicity when treated with Cet-PTXL *O*-CMC Nps compared to MIAPaCa-2 cells. PTXL-*O*-CMC Nps did not induce much toxicity in the cancer cells compared to Cet-PTXL *O*-CMC Nps. Thus, it is clearly evident that antibody conjugation aids in inducing more toxicity to EGFR expressing cancer cells. The IC50 values for the targeted and non-targeted nanoformulations at 24 h post treatment were A549 (40 μg/mL), A431 (25 μg/mL) and SKBR3 (25 μg/mL) and around 100 μg/mL for all the three cell lines in the case of non-targeted nanoformulations. No significant toxicity was induced in MIAPaCa-2 cell lines treated with both PTXL-*O*-CMC Nps and Cet-PTXL-*O*-CMC Nps and this confirms that Cet targeting is responsible for the higher cellular uptake and enhanced cytotoxicity of Cet conjugated nanoparticles in the EGFR positive cancer cell lines. Hence it is evident that Cet-PTXL-*O*-CMC Nps enhanced the chemotherapeutic effect by increasing the availability of PTXL toward the target cells.

Cancer cell death can be programmed (apoptosis) or non programmed (necrosis). Mechanism of cell death induced by the nanoparticles was analyzed by measuring the Annexin V/PI binding using flow cytometer. Fig. 7B shows the percentage of cell death induced by the Nps quantified using flow cytometry. Cet-PTXL-*O*-CMC Nps induced higher cell death (both apoptosis and necrosis) compared to that of non-targeted Nps. Some of the cells have entered into the necrotic stage where as some are in the apoptotic stage finally resulting in in vitro cancer cell death. Also they follow a similar pattern as that of free PTXL indicating that the targeted nanoformulation retains the anticancer effect of PTXL. It has been recognised that PTXL induce mitotic arrest resulting in apoptotic cell death at low concentration and necrosis at higher concentrations. The action of PTXL also depends upon the stage of cell cycle such that induce apoptotic cell death in G1 and S stages, but induced both apoptosis and necrosis in G2/M phase (Pei-Chin & Chien-Hui, 2005). So the toxicity results obtained from our study could be a combination of apoptotic and necrotic cell death depending upon the stage at which the cells are exposed to the released PTXL from Cet-PTXL-*O*-CMC NPs and also its concentration. The cancer cell death quantified by both flow cytometry and alamar blue assay are well correlating. The targeted nanoparticles induce enhanced toxicity in EGFR over expressing cancer cells compared to that of cancer cells with low EGFR expression.

The EGFRs are transmembrane glycoproteins formed by an extra-cellular ligand-binding domain, a transmembrane region and an intracellular tyrosine kinase domain with a regulatory carboxyl terminal segment. The N-terminal extra-cellular portion of EGFR can bind a variety of ligands such as EGF, TGF-β (Vincenzi et al., 2008). Receptor dimerization activates the intracellular tyrosine kinase region of EGFR, resulting in autophosphorylation and initiation of a cascade of intracellular events. The effect of these events is the recruitment and phosphorylation of several intracellular substrates with the binding of adaptor molecules to specific phosphotyrosine sites on receptor molecules. The Ras–Raf–MAPK, PI3K-AKT, JAK/STAT systems are the major downstream signaling pathways implicated. The activation of these pathways starts several transcriptional programs that mediate a variety of cellular responses, including cell division, motility, invasion, adhesion, cellular repair and survival (or death). After signal transduction, receptors can be internalized and either down-regulated or regenerated on the cell surface (Vincenzi et al., 2008). It can be hypothesized that this will block the downstream signaling cascade. The complex will be endocytosed and undergo lysosmal degradation resulting in the release of PTXL. PTXL binds the microtubules and causes kinetic suppression (stabilization) of microtubule dynamics. This suppression of microtubule dynamics inhibit formation of mitotic spindles, resulting in an arrest at G_2/M phase of the cell cycle. Studies also suggested that cells in G_2/M phase undergo cell membrane disruption followed by the leakage of LDH and other growth inhibitory substances from the cells upon PTXL treatment. In short a study in human leukemic U937 cells.paclitaxel induces typical apoptosis in the G1- and S-cells, but it induces both apoptosis and necrosis in G2/M-phase cells (Pei-Chin & Chien-Hui, 2005; Wang, Wang, & Soong, 2000). Hence, the cascade of events induced by nano drugs start with the receptor mediated endocytosis, which brings forth enhanced drug efficacy and thereby cell death at lower drug doses.

4. Conclusions

The study reported a targeted nanoformulation for the delivery of hydrophobic anticancer drug, PTXL toward EGFR over expressing cancer cells. *O*-CMC based nanoparticles prepared via simple ionic gelation technique showed to be advantageous in holding 75% of hydrophobic taxane (PTXL) and also provide carboxyl functionality for further antibody conjugation. Our preparation process resulted in spherical 200 nm sized stable particles that can be tuned within the optimal range used for drug delivery application. In vitro drug release profile shows a slow controlled and sustained release of the drug as a result of which 70–80% PTXL was released within 10 days. 80% of cell death was observed in A549, A431 and SKBR3 cancer cell lines exposed to Cet-PTXL-*O*-CMC Nps. The cellular uptake of the targeted nanoparticles analyzed qualitatively by fluorescent microscopy and quantitatively by flow cytometry showed enhanced uptake by EGFR over-expressed cancer cell lines indicating receptor based active targeting. The above results can be concluded to the fact that antibody conjugated targeted nanoparticles exhibits better selectivity for targeting cancer cells and contributed to the enhanced cancer cell death. This suggests that Cet-PTXL-*O*-CMC Nps could be used for the potential targeted delivery of PTXL toward EGFR overexpressing cancers.

Acknowledgments

This work was supported by International Division, Department of Science and Technology, Government of India and Portuguese Science Foundation (FCT), Portugal providing financial support under Indo-Portugal Joint Research Program (Ref. No. INT/PORTUGAL/P-05/2009). The work was also partially supported by Nanomission, Department of Science and Technology under a “Theragnostics” grant. The author *Maya S* was supported by Senior Research Fellowship from CSIR (SRF Award No.: 9/963 (00172)2K11-EMR-I). The authors are also thankful to Mr. Sajin. P. Ravi, Mr. Sarath and Mrs. P. R. Sreerekha for their helps in SEM and flow cytometry studies.

References

Agüeros, M., Zabaleta, V., Espuelas, S., Campanero, M. A., & Irache, J. M. (2010). Increased oral bioavailability of paclitaxel by its encapsulation through complex formation with cyclodextrins in poly(anhydride) nanoparticles. *Journal of Controlled Release*, *145*, 2–8.

Anitha, A., Chennazhi, K. P., Nair, S. V., & Jayakumar, R. (2012). 5-Flourouracil loaded *N, O*-carboxymethyl chitosan nanoparticles as an anticancer nanomedicine for breast cancer. *Journal of Biomedical Nanotechnology*, *8*, 1–14.

Anitha, A., Divyarani, V. V., Krishna, R., Sreeja, V., Selvamurugan, N., Nair, S. V., et al. (2009). Synthesis, characterization, cytotoxicity and antibacterial studies

of chitosan, *O*-carboxymethyl and *N*, *O*-carboxymethyl chitosan nanoparticles. *Carbohydrate Polymers*, *78*, 672–677.
Anitha, A., Maya, S., Deepa, N., Chennazhi, K. P., Tamura, H., Nair, S. V., et al. (2011). Efficient water soluble *O*-carboxymethyl chitosan nanocarrier for the delivery of curcumin to cancer cells. *Carbohydrate Polymers*, *83*, 452–461.
Bareford, L. M., & Swaan, P. W. (2007). Endocytic mechanisms for targeted drug delivery. *Advanced Drug Delivery Reviews*, *59*, 748–758.
Barnard, J. A., Beauchamp, J., Russell, W. E., DuBois, R. N., & Coffey, R. J. (1995). Epidermal growth factor-related peptides and their relevance to gastrointestinal pathophysiology. *Gastroenterology*, *108*, 564–580.
Benhabbour, S. R., Luft, J. C., Kim, D., Jain, A., Wadhwa, S., Parrott, M. C., et al. (2012). In vitro and *in vivo* assessment of targeting lipid-based nanoparticles to the epidermal growth factor-receptor (EGFR) using a novel heptameric ZEGFR domain. *Journal of Controlled Release*, *158*, 63–71.
Courrier, H. M., Butz, N., & Vandamme, T. F. (2002). Pulmonary drug delivery systems: Recent developments and prospects. *Critical Reviews in Therapeutic Drug Carrier Systems*, *19*, 425–498.
Dass, C. R., & Su, T. (2001). Particle-mediated intravascular delivery of oligonucleotides to tumors: Associated biology and lessons from genotherapy. *Drug Delivery*, *8*, 191–213.
Deepagan, V. G., Sarmento, B., Menon, D., Nascimento, A., Jayasree, A., Sreeranganathan, M., et al. (2012). In vitro targeted imaging and delivery of camptothecin using cetuximab conjugated multifunctional PLGA-ZnS nanoparticles. *Nanomedicine*, *7*, 507–519.
Dutta, P. K., & Dey, J. (2011). Drug solubilization by amino acid based polymeric nanoparticles: Characterization and biocompatibility studies. *International Journal of Pharmaceutics*, *421*, 353–363.
Gareth, H. (2005). Nanostructure-mediated drug delivery. *Nanomedicine: Nanotechnology Biology and Medicine*, *1*, 22–30.
Gullick, W. J. (1991). Prevalence of aberrant expression of the epidermal growth factor receptor in human cancers. *British Medical Bulletin*, *47*, 87–98.
Gupta, V. K., Karar, P. K., Ramesh, S., Misra, S. P., & Gupta, A. (2010). Nanoparticle formulation for hydrophilic & hydrophobic drugs. *International Journal of Research in Pharmaceutical Sciences*, *1*, 163–169.
Huang, Z., Tang, Y., Zhou, X., Zhou, Y., Jin, D., Li, Y., et al. (2012). Magnetic micelles as a potential platform for dual targeted drug delivery in cancer therapy. *International Journal of Pharmaceutics*, *429*, 113–122.
Jayakumar, R., Prabaharan, M., Nair, S. V., Tokura, S., Tamura, H., & Selvamurugan, N. (2010). Novel carboxymethyl derivatives of chitin and chitosan materials and their biomedical applications. *Progress in Materials Science*, *55*, 675–709.
Jin, H., Lovell, J. F., Chen, J., Ng, K., Cao, W., Ding, L., et al. (2010). Investigating the specific uptake of EGF-conjugated nanoparticles in lung cancer cells using fluorescence imaging. *Cancer Nanotechnology*, *1*, 71–78.
Kirkpatrick, P., Graham, J., & Muhsin, M. (2004). Cetuximab. *Nature Reviews Drug Discovery*, *3*, 549–550.
Lakshmanan, V. K., Snima, K. S., Bumgardner, J. D., Nair, S. V., & Jayakumar, R. (2011). Chitosan based nanoparticles in cancer therapy. *Advances in Polymer Science*, *243*, 55–91.
LaVan, D. A., Lynn, D. M., & Langer, R. (2002). Moving smaller in drug discovery and delivery. *Nature Reviews Drug Discovery*, *1*, 77–84.
LaVan, D. A., McGuire, T., & Langer, R. (2003). Small-scale systems for *in vivo* drug delivery. *Nature Biotechnology*, *21*, 1184–1191.
Lee, H., Fonge, H., Hoang, B., Reilly, R. M., & Allen, C. (2010). The effects of particle size and molecular targeting on the intratumoral and subcellular distribution of polymeric nanoparticles. *Molecular Pharmaceutics*, *7*, 1195–1208.
Li, F., Li, J., Wen, X., Zhou, S., Tong, X., Su, P., et al. (2009). Anti-tumor activity of paclitaxel-loaded chitosan nanoparticles: An *in vitro* study. *Materials Science and Engineering: C*, *29*, 2392–2397.
Li, S., Schmitz, K. R., Philip, D. J., Jed, J. W., Wiltzius, Kussie, P., et al. (2005). Structural basis for inhibition of the epidermal growth factor receptor by cetuximab. *Cancer Cell*, *7*, 301–311.
Liao, C., Sun, Q., Liang, B., Shen, J., & Shuai, X. (2011). Targeting EGFR-over expressing tumor cells using Cetuximab-immunomicelles loaded with doxorubicin and superparamagnetic iron oxide. *European Journal of Radiology*, *80*, 699–705.
Löw, K., Wacker, M., Wagner, S., Langer, K., & von Briesen, H. (2011). Targeted human serum albumin nanoparticles for specific uptake in EGFR-expressing colon carcinoma cells. *Nanomedicine*, *7*, 454–463.
Marciniak, D. G., Moragoda, L., Mohammad, R. M., Yu, Y., Nagothu, K. K., Aboukameel, A., et al. (2003). Epidermal growth factor receptor-related protein: A potential therapeutic agent for colorectal cancer. *Gastroenterology*, *124*, 1337–1347.
Maya, S., Indulekha, S., Sukhithasri, V., Smitha, K. T., Nair, S. V., Jayakumar, R., et al. (2012). Efficacy of tetracycline encapsulated *O*-carboxymethyl chitosan nanoparticles against intracellular infections of *Staphylococcus aureus*. *International Journal of Biological Macromolecules*, *51*, 392–399.
Mickler, F. M., Mockl, L., Ruthardt, N., Ogris, M., Wagner, E., & Brauchle, C. (2012). Tuning nanoparticle uptake: Live-cell imaging reveals two distinct endocytosis mechanisms mediated by natural and artificial EGFR targeting ligand. *Nano Letters*, *12*, 3417–3423.
Pei-Chin, L., & Chien-Hui, L. (2005). Cell cycle specific induction of apoptosis and necrosis by paclitaxel in the leukemic U937 cells. *Life Sciences*, *76*, 1623–1639.
Pirker, R., & Filipits, M. (2010). Monoclonal antibodies against EGFR in non-small cell lung cancer. *Critical Reviews in Oncology/Hematology*, *80*, 1–9.
Prabaharan, M., Reis, R. L., & Mano, J. (2007). Carboxymethyl chitosan-graft-phosphatidylethanolamine: Amphiphilic matrices for controlled drug delivery. *Reactive and Functional Polymers*, *67*, 43–52.
Ravi Kumar, M. N. V., Muzzarelli, R. A. A., Muzzarelli, C., Sashiwa, H., & Domb, A. J. (2004). Chitosan chemistry and pharmaceutical perspectives. *Chemical Reviews*, *104*, 6017–6084.
Reid, A., Vidal, L., Shaw, H., & Bono, J. (2007). Dual inhibition of ErbB1 (EGFR/HER1) and ErbB2 (HER2/neu). *European Journal of Cancer*, *43*, 481–489.
Sanoj, R. N., Muthunarayanan, M., Divyarani, V. V., Sreerekha, P. R., Chennazhi, K. P., Nair, S. V., et al. (2011). Curcumin-loaded biocompatible thermo-responsive polymeric nanoparticles for cancer drug delivery. *Journal of Colloids and Interface Science*, *360*, 39–51.
Senior, K. B. (1998). Nano-dumpling with drug delivery potential. *Molecular Medicine Today*, *4*, 321.
Snima, K. S., Jayakumar, R., Unnikrishnan, A. G., Nair, S. V., & Lakshmanan, V. K. (2012). O-carboxymethyl chitosan nanoparticles for metformin delivery to pancreatic cancer cells. *Carbohydrate Polymers*, *89*, 1003–1007.
Ulbrich, K., & Subr, V. (2004). Polymeric anticancer drugs with pH-controlled activation. *Advanced Drug Delivery Reviews*, *56*, 1023–1050.
Vincenzi, B., Schiavon, G., Silletta, M., Santini, D., & Tonini, G. (2008). The biological properties of cetuximab. *Critical Reviews in Oncology/Hematology*, *68*, 93–106.
Wang, T., Wang, H., & Soong, Y. (2000). Paclitaxel induced cell death. *Cancer*, *88*, 2619–2628.
Zielinski, C. (2006). Potential of biologically targeted therapies for breast cancer. *EJC Supplements*, *4*, 23–26.